

# Can a “pre-worn” bearing surface geometry reduce the wear of metal-on-metal hip replacements? – A numerical wear simulation study

Leiming Gao<sup>a,\*</sup>, Zikai Hua<sup>b</sup>, Robert Hewson<sup>a</sup>

<sup>a</sup> Department of Aeronautics, Imperial College London, London SW7 2AZ, UK

<sup>b</sup> School of Mechatronics Engineering and Automation, Shanghai University, Shanghai 200444, China

## ARTICLE INFO

### Keywords:

Total Hip Replacement (THR)  
Metal-on-metal  
Non-spherical  
Worn geometry  
Wear simulation  
EHL

## ABSTRACT

Total Hip Replacement (THR) is generally a highly successful treatment for late stage hip joint diseases and wear, however, wear continues to be one of the major causes of metal-on-metal THR's failure. Hip replacements typically experience a two-stage wear; a higher initial wear rate in the beginning followed by a lower steady-state one with the surface profile changed. This alludes to the potential use of a cup with a non-spherical interior cavity with an initial geometry similar to a worn surface which may benefit from lower wear rate. In this paper wear is numerically simulated with a cup having a non-spherical geometry inspired by the initial stage of wear.

A wear model was recently developed by the authors for the THR, which considered the lubricated contact in both elastohydrodynamic lubrication (EHL) and mixed lubrication regime, rather than a dry contact used in most of other studies of wear modelling in the academic literature. In this study the wear model has been updated by introducing the ‘λ ratio’ (the ratio of film thickness to surface roughness) and addressing the non-Newtonian shear-thinning properties of the synovial fluid. This wear model was able to describe the non-linear wear evolution process due to the change of worn profiles. Firstly the wear of a spherical hip joint was simulated until a steady-state wear rate is achieved. Then a non-spherical joint was proposed in which the cup bearing geometry was generated by the previously predicted worn profile from the spherical joint. At last the wear of this “pre-worn” hip bearing was simulated and compared to the spherical one. Approximately 40% reduction in the steady-state wear rate and 50% in the total accumulated wear has been observed in the non-spherical hip joint. This study presented a full numerical analysis of the relationship between lubrication, wear reduction and the geometry change, and quantitatively suggested the optimal geometry to reduce running-in wear.

## 1. Introduction

Total Hip Replacement (THR) is generally a highly successful treatment for joint diseases, however, wear and wear products (wear particles, corrosion products and metal ions) continuous to be one of the major causes of metal-on-metal (MoM) THR's failure [1]. There is dramatic drop in the clinical use of MoM implants, although they are still used in some selected patient populations, particularly the younger and more active one, with apparent success [2–4]. The wear of metal surfaces can be very low thanks to the improved techniques in material and manufacturing nowadays. However, unlike the bearing couples operating in machines which are assembled with accurate position, the wear of MoM hip bearings can be quite high under adverse operating conditions, such as edge loading due to improper positioning or design. Furthermore, the metal wear products are nanometres in size and high in numbers, and may migrate through the joint capsule to the human body and cause of long-term metal toxicity [5]. The released metal wear

particles can also have adverse biological reactions with the soft tissues around the joint, for example, 'pseudo-tumours' found in patients associated with high metal ion levels in metal-on-metal joint bearings [6]. Thus to reduce wear and wear particles are important to improve the reliability of the MoM hip implants. This paper proposes an idea that small changes to the surface geometry of MoM hip implants might reduce their cumulative revision rates enough to make them a viable option to a wider group of patients.

The shape of the joint bearing surfaces plays a key role in the kinematics and lubrication performance, which affect the level of wear. The natural hip is often referred to as spherical ball and socket joint, however their shape is deviate from a sphere [7]. Menschik [8] found that the rotational conchoids with the general formula,

$$r = a + b \cdot \cos\phi \quad (1)$$

described the hip joint geometry better than a sphere for both osseous and cartilage shapes, by measurements of normal natural hip joints,

\* Corresponding author.

E-mail address: [leiming.gao@imperial.ac.uk](mailto:leiming.gao@imperial.ac.uk) (L. Gao).

<https://doi.org/10.1016/j.wear.2018.03.010>

Received 12 October 2017; Received in revised form 6 February 2018; Accepted 18 March 2018

Available online 20 March 2018

0043-1648/ © 2018 The Authors. Published by Elsevier B.V. This is an open access article under the CC BY-NC-ND license (<http://creativecommons.org/licenses/by-nc-nd/4.0/>).

where  $r$  and  $\varphi$  are spherical coordinates;  $a$  and  $b$  are parameters. Gu et al. [9] compared the contact stress among the natural hip, a rotational ellipsoid and a sphere hip using Finite Element (FE) contact models, and concluded that the non-spherical shape contributed to optimal and more evenly distributed contact stress than the spherical one.

Although evolution has resulted in non-spherical geometry for cartilage-on-cartilage hip joints, it is not assured as the best choice for artificial hips with different material combinations and lubrication mechanics. Thus majority of the designs for hip replacements have a spherical shape apart from the non-sphericity due to manufacture tolerances or micro-scale surface roughness. However, some theoretical studies have reported the potential benefit of non-spherical shape for hip replacements in terms of lubrication and contact stress. Wang et al. [10] presented a transient Elastohydrodynamic Lubrication (EHL) simulation of ellipsoidal cup and a spherical head and concluded that proper changes in the axial radii of the ellipsoidal cup was beneficial to the EHL pressure and film thickness. Meng et al. [11] presented a dry contact and steady-state EHL analysis of an Alparabola cup, as described by Eq. (2), on a spherical head whose geometry was proposed by Fisher [12].

$$\frac{x^2}{R^2/\alpha} + \frac{(y - R + R/\alpha)^2}{R^2/\alpha^2} + \frac{z^2}{R^2/\alpha} = 1 \quad (2)$$

where,  $x$ ,  $y$  and  $z$  are Cartesian coordinates,  $R$  is the minimum curvature radius of the cup bearing surface, and  $\alpha$  is the Alparabola parameter which is close but less than 1. Gao et al. [13] further investigate the transient EHL simulation of this Alparabola hip in walking cycles. Both studies of the Alparabola shape of hip joints found better lubrication performance compared to the spherical shape, with thicker lubricated film, lower peak pressure (or contact stress for the dry contact model) and larger lubricated area. The relationship between wear reduction and the increase of contact area has been studied using Herzian contact FE models [14]. Lippincott and Medley [15] proposed another patent in which they discussed ways to create the pre-worn metal surface, in addition, to sculpt the worn surfaces to improve the lubrication paying particular attention to the inlet zone. This concept was further developed by the specification of multiple radii of curvature in the DePuy aSphere™ MoM implant, and the wear reduction were reported by the physical hip simulator tests [16,17].

A few hip simulator studies have inspired the idea that the design of proper non-spherical shape benefits to the wear reduction of the hip joints due to the nature of the ‘two-stage’ wear [18–21]. The ‘two-stage’ wear performance has typically been observed in many clinical and hip simulator studies of hip joints despite of material combinations, bearing size or clearance; a higher initial wear rate in the beginning, named the ‘running-in’ or ‘bedding-in’ period, followed by a much lower ‘steady-state’ one with the surface profile changed. This surface profile change alludes to the potential use of a cup component with a non-spherical interior cavity with an initial geometry similar to a worn surface which may benefit from better lubrication and lower wear rate. However, complete simulations of the wear performance of pre-defined non-spherical hip joints in walking cycles, neither in physical hip simulator or numerical analysis, have not been reported to the best of our knowledge. The current study is aiming to numerically investigate the wear of a specially designed non-spherical MoM hip joint and its potential benefit to get rid of high wear rate in the ‘running-in’ wear stage. First of all, a proper wear model is required to be able to simulate the two-stage wear process. A brief literature review on the wear models are presented in the following.

In the literature of wear modelling of hip joint replacements, the Archard wear law [22] has been commonly used [23–36]. For the hard-on-hard hip joints, namely metal-on-metal, ceramic-on-metal or ceramic-on-ceramic hips, the linear wear depth is proportional to the local contact stress and sliding distance, through a wear coefficient. For hard-on-soft materials, namely metal (ceramic)-on-plastic, the linear

wear is also dependent to the multi-directional motion which resulting in the cross-shear effect. There are various methods regarding the calculation of the cross-shear ratio and furthermore, how to define the wear factor as a function of the cross-shear ratio [33,37]. Most of the wear models were based on a dry contact simulation without addressing the lubrication explicitly. Instead, lubrication effect was addressed in the wear factor which is empirically derived. When the dry contact stress been applied to the Archard wear law an almost constant wear rate against time was obtained as the total force applied to the joint is the same in each cycle resulting in the integration of the contact stress over contact area (that contributes the wear volume) per cycle being constant. As such the predicted wear does not replicate the two-stage trend if the wear factor is set. In the academic literature, most wear models of metal-on-metal hip joints employed two constant wear factors, one representing for the running-in stage and another for the steady-state stage, with the values typically residing in a wide range of the order of magnitude of  $10^{-9}$ – $10^{-8}$  mm<sup>3</sup>/(N m) [24,27,31,32,34,36].

There are some studies that evaluated wear factors with consideration of specific loading conditions, lubrication performance, and surface roughness, rather than using constant values. Di Puccio and Mattei [32,34,38] derived the wear coefficients from experimental measurements, separately for each rubbing component such as the cup and head component in hip joint replacements. Their model reconstructed the worn profiles at the cup and head surfaces, and highlighted that a single wear coefficient was not accurate if both surfaces undergoes wear, and need to be derived from the wear testing data for specific tribology system. Pakhaliuk et al. [35] proposed wear factor as a power function of the contact pressure, using different power to distinguish the two wear stages. Harun et al. [36] curve fitted a single wear factor formula as a power function of the ‘lambda ratio’ (ratio of the minimum film thickness to the composite average surface roughness) from experimental tests among various head sizes and diametrical clearances. Their work highlighted the role of lubrication in wear through one statistical lambda ratio, while only the linear wear rate was presented for the hip joints wear. Wang et al. [39] reported an exponential relationship between the wear factor and average roughness from physical hip simulator tests. Hall et al. [40] also found similar relationship from clinical retrieved acetabular cups. Recently a new wear model of lubricated hip joints was developed by the authors [28] which addressed the mixed and elastohydrodynamic lubrication in full pressure and film thickness field. The wear coefficient was proposed as a power function of the local film thickness and the average surface roughness, which is time dependent. By considering the full lubrication analysis in wear, the two-stage wear evolution was successfully obtained, and detailed wear profiles for separate cup and head surfaces were observed as well.

In this study, a non-spherical metal-on-metal hip joint was proposed and the wear performance was simulated and compared with the spherical hip. The non-Newtonian (shear-thinning) property of the synovial fluid is addressed in the lubrication model. Firstly wear of a spherical joint is simulated for two million cycles to achieve a steady-state wear stage. Then the predicted worn profiles on both the cup and head bearing surfaces are used to numerically create a general ‘pre-worn’ cup geometry.

## 2. Geometry, materials and loading cycles

A spherical metal-on-metal (CoCrMo) total hip replacement was firstly studied, having the diameter of 36 mm and radial clearance of 25 μm. The cup was positioned against the head component with an inclination angle of 45°. An equivalent layer representing the bone and/or fixation was placed outside to the cup component. After completing the wear simulation of this spherical hip joint, the total worn geometry (included wear of both the cup and head bearing surfaces) was fitted to a rotational Gaussian surface by finding the parameter  $d$  and  $\sigma$  in spherical coordinates,

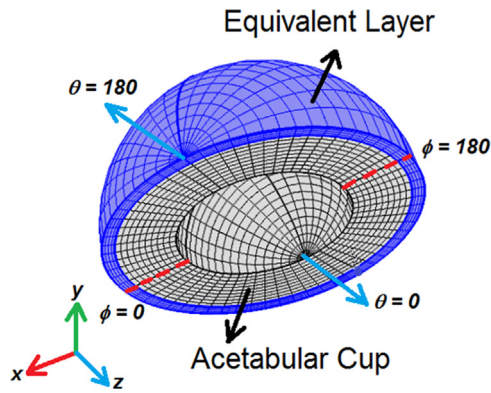


Fig. 1. Illustration of an acetabular cup for lubrication and wear modelling.

$$f(\varphi, \theta) = d \times \exp[-0.5 \times [(\varphi - \varphi_0)^2 + (\theta - \theta_0)^2] / \sigma^2] \quad (3)$$

where  $\varphi$  and  $\theta$  are spherical coordinates,  $\varphi_0$  and  $\theta_0$  are coordinates at the centre of dimple,  $d$  represents the maximum radial change from the spherical geometry,  $\sigma$  represents the radius of area that are modified from spherical geometry. This numerically generated surface was then applied to the cup bearing surface to create a new ‘pre-worn’ non-spherical profile, while the head component was kept spherical given consideration to the simplification of design and manufacture. For both joints, the cup was inclined and fixed to the pelvic bone through an equivalent layer representing bone and/or fixation cement, as illustrated in Fig. 1. The material and geometrical parameters are presented in Table 1 [28]. The radial clearance is defined as the radius of curvature of the spherical surfaced cup minus the radius of curvature of the spherical surfaced head before any wear occurs.

The loading and motion pattern of gait cycles employed in ProSim hip simulators [41,42] was considered in this study, as shown in Fig. 2, the cup component moves in the flexion-extension direction and the head moves in the internal-external rotation.

### 3. Wear model

The current wear model was developed based on the authors' previous wear model [28]. As the hip replacements operate in a mixed lubricated regime, the level of wear depends on the film thickness and the bearing surface roughness apart from the contact stress and sliding distance, and the wear resistance of rubbing materials. Thus, the ‘ $\lambda$  ratio’ of the film thickness ( $h$ ) to the average composite roughness ( $R_a$ ), was introduced here. In lubrication analysis the  $\lambda$  ratio is an index for assessment of lubrication modes. In general,  $\lambda \leq 1$  suggests boundary lubrication while  $\lambda = 1-2$  mixed lubrication and  $\lambda \geq 3$  full fluid film lubrication. In the full film lubrication regime ( $\lambda \geq 3$ ), the wear rate is zero, which is updated from the author's previous model [28]. The linear wear rate, i.e. wear depth per unit time, from the implant bearing surfaces was described as:

$$\text{wear rate} = \begin{cases} k_w p v (1/\lambda)^a, & \text{if } \lambda < 3 \\ 0, & \text{if } \lambda \geq 3 \end{cases} \quad (4)$$

Table 1

Geometrical and material parameters of a MOM THR.

Radial clearance	25 $\mu\text{m}$
Head radius, $R$	18 mm
Cup wall thickness	9.5 mm
Equivalent support thickness	2 mm
Elastic modulus of metal	210 GPa
Elastic modulus of equivalent support layer	2.27 GPa
Poisson's ratio of metal	0.3
Poisson's ratio of equivalent support layer	0.23

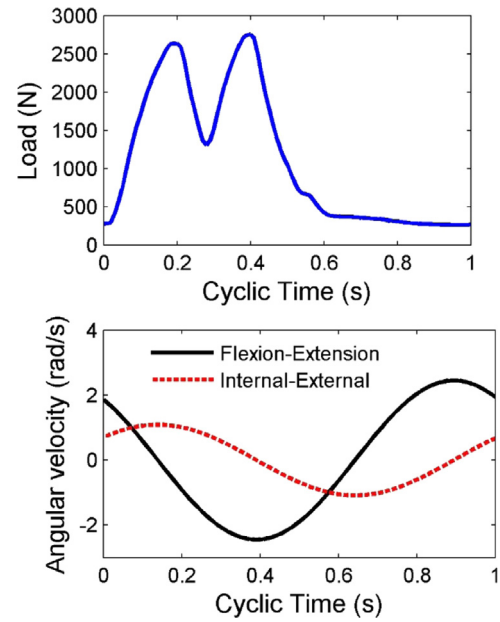


Fig. 2. Load and angular velocity of ProSim hip simulator in gait cycle.

$$\lambda = h/R_a \quad (5)$$

where  $k_w$  is a constant wear parameter related to wear resistance of the metal material,  $p$  is the fluid pressure, and  $v$  is the local relative sliding speed of the two surfaces. This makes the wear law remain a uniform expression with the working conditions spanning from the boundary to full film lubrication regimes. The power term ( $a$ ) determines how sensitive the transition to wear changes with a decreasing film thickness, and its value of 2.24 was used here which was found reasonably capture the surface wear of metal gears [43] and metal-on-metal hips [28]. As the surface roughness of hip components made of CoCrMo alloy are in the range of 16–50 nm [42], a composite average surface roughness of 40 nm of hip bearing surfaces was employed.

It needs to be noted that the wear was simulated on the cup and head components separately at each time step. The two motions were simulated simultaneously as the flexion-extension of the cup component and the internal-external rotation on the head. Wear on the cup surface was calculated on the cup mesh frame, and wear on the head was undertaken on the head frame. Since the lubrication mesh was fixed on the cup frame, the wear of cup was calculated straight away using the pressure and film thickness obtained from the lubrication solution and the sliding speed of the cup mesh. While for the head component, at each time step (apart from the initial one when the mesh of the two bearing surfaces were overlapped), the lubrication solution (pressure and film thickness) and sliding speed were interpolated onto the head frame to find the corresponding values for each mesh point. For convenient presentation the separate wear on cup or head frames were not noted separately in the following equations. The linear wear ( $W_L^{ij}$ ) at random mesh point ( $i, j$ ) at the  $k^{\text{th}}$  time step in a gait cycle was derived as

$$W_L^{ij}(k) = k_w p_{i,j} v_{i,j} \Delta t (R_a/h_{i,j})^a; i = 1, \dots, m; j = 1, \dots, m; k = 1, \dots, n \quad (6)$$

where,  $\Delta t$  is the discrete time step in an evenly time mesh distribution;  $m$  is the number of mesh grid ( $m = 256$ ) in each  $\theta$  and  $\varphi$  coordinate; there were  $n = 100$  time steps in one gait cycle. The discrete relative sliding speed was calculated as a composite of two velocity components in spherical coordinates:

$$v = \sqrt{v_\theta^2 + v_\varphi^2} \quad (7)$$

$$\begin{cases} v_\theta = -R\omega_x \sin\varphi + R\omega_y \cos\varphi \\ v_\varphi = -R\omega_x \cos\varphi \cos\theta - R\omega_y \sin\varphi \cos\theta \end{cases} \quad (8)$$

where,  $R$  is the radius of the cup bearing surface;  $\omega_x$ ,  $\omega_y$  represent the angular speed for the flexion-extension and internal-external rotation respectively. The wear depth at point  $(i, j)$  was summed over all time steps ( $n$ ) in one cycle,

$$W_{L,cyc}^{ij} = \sum_{k=1}^n W_L^{ij}(k) \quad (9)$$

The wear depth at each point  $(i, j)$  during  $N$  gait cycles can be approximately evaluated as the number of cycles multiply the wear depth per cycle, if the change of surface profile was not large enough to affect the lubrication within  $N$  cycles.

$$W_{L,tot}^{ij} = \sum_1^N W_{L,cyc}^{ij} \approx N \cdot W_{L,cyc}^{ij} \quad (10)$$

After a designed number of cycles the changes of surface profile became large enough to affect the lubrication film thickness and pressure fields, thus the surface needed to update before continuing the simulation. The update was then input into the film thickness equation in the EHL model below.

The accumulated wear was calculated as a sum of the volumetric wear at all mesh cells (total number of  $m = 256$  in each spherical coordinate) over the bearing surface. The volumetric wear at each mesh cell was calculated as the product of the linear wear and the area of the mesh cell ( $A$ ) with that point at the centre,

$$W_{vol} = \sum_{i=1}^m \sum_{j=1}^m (W_{L,tot}^{ij} \times A_{ij}) \quad (11)$$

$$A_{ij} \approx (\pi R/m)^2 \cdot \sin\theta_{ij} \quad (12)$$

A flowchart describing the wear simulation procedure can be found in Ref. [28].

#### 4. EHL model

The EHL model has been accounted for the non-Newtonian shear-thinning characteristics of the synovial fluid. However, the role of protein aggregation in transporting with fluid in the rheology model has not been addressed, which is a limitation of the current model. The Reynolds equation was used to describe the synovial flow in hip replacements formulated in spherical coordinates [44,45]:

$$\begin{aligned} & \frac{\partial}{\partial\varphi} \left( \frac{h^3}{\eta} \frac{\partial p}{\partial\varphi} \right) + \sin\theta \frac{\partial}{\partial\theta} \left( \frac{h^3}{\eta} \sin\theta \frac{\partial p}{\partial\theta} \right) \\ & = 6R^2 \sin\theta \left[ -\omega_x \left( \sin\varphi \sin\theta \frac{\partial h}{\partial\theta} + \cos\varphi \cos\theta \frac{\partial h}{\partial\varphi} \right) \right. \\ & \quad \left. + \omega_y \left( \cos\varphi \sin\theta \frac{\partial h}{\partial\theta} - \sin\varphi \cos\theta \frac{\partial h}{\partial\varphi} \right) \right] \\ & \quad + 12R^2 \sin^2\theta \frac{\partial h}{\partial t} \end{aligned} \quad (13)$$

Considering the angle of cup inclination ( $\beta$ ), the calculation domain of the lubrication was defined as  $\theta = [0, \pi]$  and  $\varphi = [\beta, \beta + \pi]$ . At both inlet and the outlet boundaries (boundaries of the calculation domain) the hydrodynamic pressure ( $p$ ) was set to be zero. For the cavitation boundary condition, negative pressure, once obtained during the relaxation process, was set to zero immediately. The shear-thinning property of synovial fluid was described by the Cross formula [46].

$$\eta = \eta_\infty + (\eta_0 - \eta_\infty) / [1 + \alpha(\dot{\gamma})^\beta] \quad (14)$$

The values of viscosity at limiting shear rate were ( $\eta_0 = 40,000$  mPa s) and ( $\eta_\infty = 0.9$  mPa s). The parameters in the formula

was given with  $\alpha = 9.54$  and  $\beta = 0.73$ . These values of viscosity for synovial fluid were observed from eight different sources suggested that a fair representation of viscosity over a large range of shear rates encountered in joint replacements [47]. The pressure change across the lubricating film thickness direction was ignored because of the very thin films in EHL regime. The average shear rate ( $\dot{\gamma}$ ) was calculated as the ratio of relative surface velocity to film thickness.

$$\dot{\gamma} = v/h \quad (15)$$

The film thickness ( $h$ ) was calculated in three parts; the rigid gap between the two bearing surfaces which included the radial clearance of the cup and head ( $c$ ), and three eccentricity components ( $e_{x,y,z}$ ); the elastic deformation ( $\delta$ ) of the surfaces; and the non-spherical change in the cup inside surface ( $f$ ),

$$h(\varphi, \theta) = c - e_x \sin\theta \cos\varphi - e_y \sin\theta \sin\varphi - e_z \cos\theta + \delta(\varphi, \theta) + f(\varphi, \theta) \quad (16)$$

$$\delta(\varphi, \theta) = \int_\varphi \int_\theta K(\varphi - \varphi', \theta - \theta', \theta_m) p(\varphi', \theta') d\theta' d\varphi' \quad (17)$$

where in the elastic deformation,  $K$  denotes the influence coefficient matrix of the elastic surfaces and  $\theta_m$  denotes a fixed mean latitude. An Equivalent Spherical Discrete Convolution (ESDC) technique [48] and the Multi-Level Multi-Integration (MLMI) were adopted to obtain the surface elastic deformation [49]. When the calculated film thickness was less than a certain small value, here chosen as 20 nm physically represent the boundary film thickness, the film thickness was set to the small value [43], and the local contact pressure was derived from the film thickness equation. The applied load were balanced by the integral of the hydrodynamic/contact pressure in the three Cartesian coordinate dimensions:

$$w_{x,y,z} = R^2 \int_\varphi \int_\theta p_{x,y,z} d\theta d\varphi \quad (18)$$

where the pressure components ( $p_x, p_y, p_z$ ) in the three Cartesian directions were calculated as

$$\begin{cases} p_x = p \sin^2\theta \cos\varphi \\ p_y = p \sin^2\theta \sin\varphi \\ p_z = p \sin\theta \cos\theta \end{cases} \quad (19)$$

The governing equations were transformed to dimensionless and subsequently discrete forms in order to use the finite difference schemes. Gauss-Seidel relaxation was adopted in solving the Reynolds equation in terms of pressure iteration. The Multi-Grid technique was adopted to solve the equation system. The details of these numerical procedures can be found in Refs. [44,50].

#### 5. Results

For convenience we use the term ‘non-spherical hip’ to briefly represent the one having a spherical head against the non-spherical cup inside bearing geometry which was similar to the ‘pre-worn’ geometry. The wear of both spherical and non-spherical hip joints were simulated for two million cycles (MC). The wear coefficient of  $2 \times 10^{-8}$  mm<sup>3</sup>/(Nm) and an update interval of 25,000 cycles were employed here, to ensure independent wear results to the frequency of worn profile update, the sensitivity of this update frequency has been investigated in the author’s previous work [28]. The non-spherical profile for the cup bearing surface was described by Eq. (3) and the parameter  $d$  and  $\sigma$  was calculated as 1.25  $\mu$ m and 15° respectively (for  $\theta$  and  $\varphi$  in degrees).

The total accumulated wear volume variations in the simulated two million cycles are shown in Fig. 3, in which the head and cup surface wear are presented in upper and lower part separately. Approximately 50% reduction in the total wear was found in the non-spherical hip joint. The non-linear wear is clearly observed in the spherical joint (transformed at around the 0.75 MC), while a nearly linear wear in the

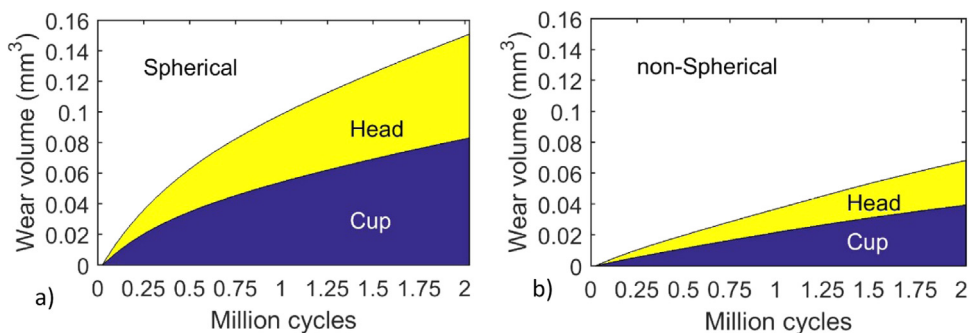


Fig. 3. Accumulated wear volume of a) spherical and b) non-spherical hip joints.

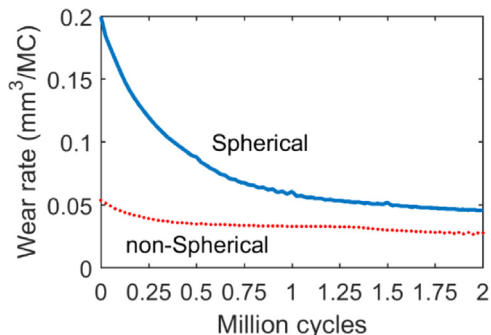


Fig. 4. Wear rate (total of cup and head) comparison between the spherical and non-spherical hip joints.

non-spherical joint during all simulated cycles. For both joints the wear of cup was slightly greater (~ 10%) than that of the head. Furthermore, the wear rates calculated from the total wear volume of the two studied joints was compared in Fig. 4. The running-in wear rate (0.08–0.2 mm<sup>3</sup>/MC) and steady-state wear rate (~ 0.05 mm<sup>3</sup>/MC) were observed in the spherical hip; while in the non-spherical hip, there was a very short transition period until around 0.25 MC, and the wear rate varied from a slightly high value of (~ 0.05 mm<sup>3</sup>/MC) to a steady-state one (~ 0.03 mm<sup>3</sup>/MC).

The wear development was presented in Figs. 5 and 6, in which each figure contains the wear contours after simulation and the wear depth distribution on the Interior-Posterior cross-section ( $\varphi = 135^\circ$ , as shown by the dash line in contours) at different cycles in the simulated wear process. The maximum wear depth was 1.04  $\mu\text{m}$  (cup) and 0.88  $\mu\text{m}$  (head) for the spherical hip joint, and 0.51  $\mu\text{m}$  (cup) and 0.27  $\mu\text{m}$  (head) for the non-spherical hip. These results are presented on the cup frame and the centre of contact is  $\varphi = 135^\circ$  rather than  $90^\circ$  because of

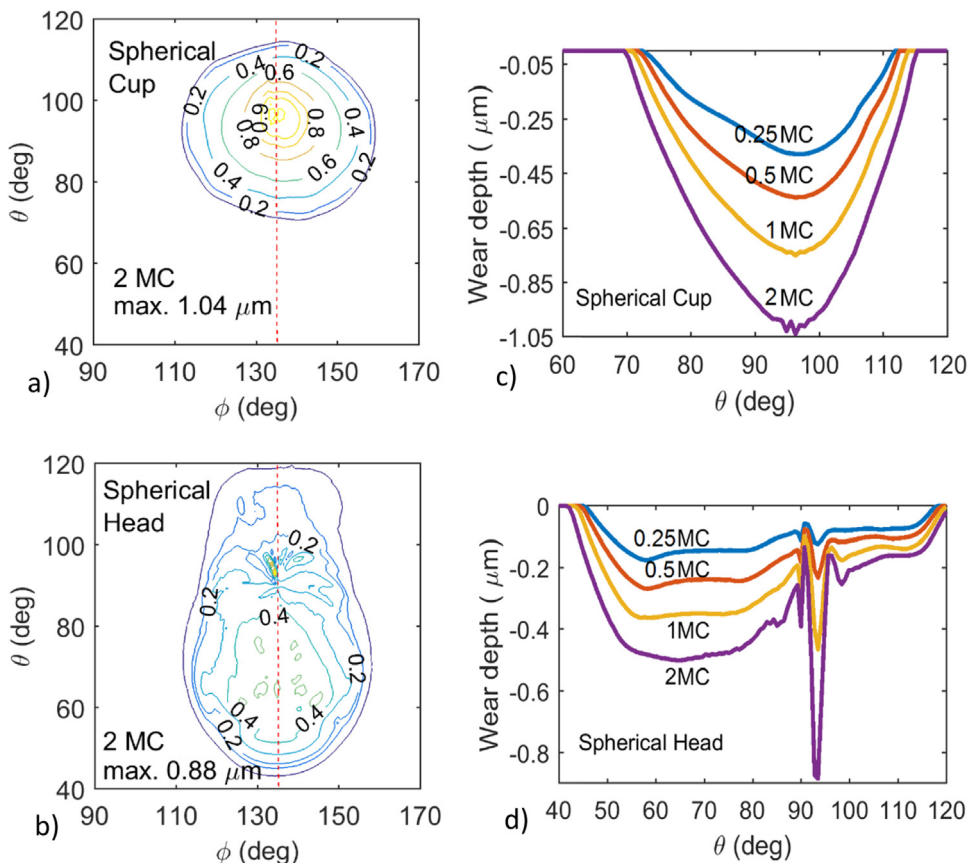


Fig. 5. Wear of the spherical hip joint: the wear scar contours after 2MCs on the bearing surface of a) cup and b) head; interior-posterior cross-section wear depth development of c) cup and d) head.

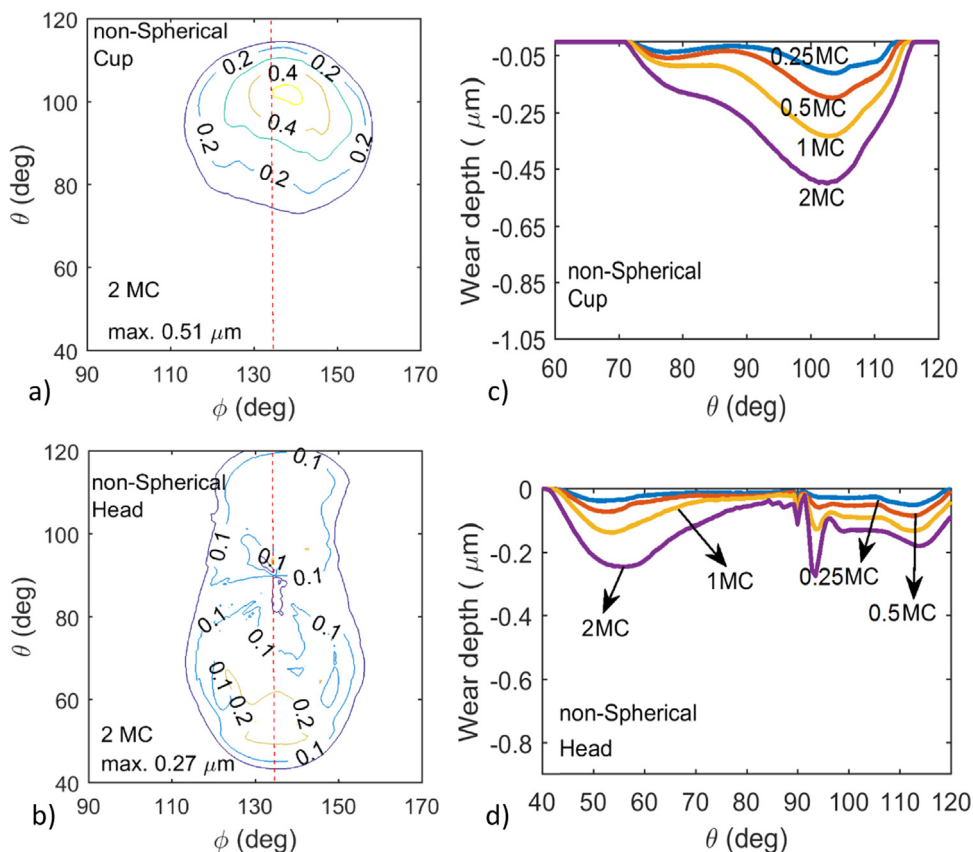


Fig. 6. Wear of the non-spherical hip joint: the wear scar contours after 2MC on the bearing surface of a) cup and b) head; interior-posterior cross-section wear depth development of c) cup and d) head.

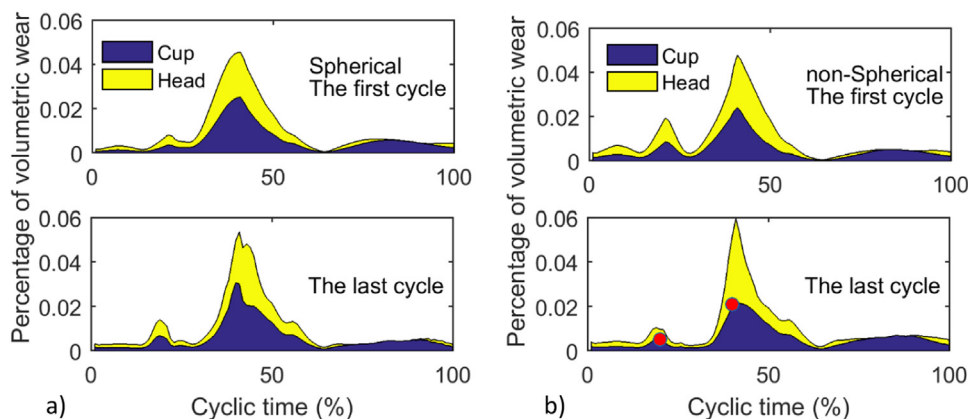


Fig. 7. Volumetric wear variations against time in one gait cycle (the wear of head was added on the top of the cup wear); a) the spherical hip; b) the non-spherical hip with red dots indicate the cup wear at 20% and 40% of the last wear cycle. (For interpretation of the references to color in this figure legend, the reader is referred to the web version of this article.)

an inclination angle of cup of 45°.

In order to find out the effect of loading cycles on the wear performance, the percentage of volumetric wear in two cycles is presented in Fig. 7, the first and the last walking cycle of the total wear simulation. The ‘percentage’ here means that the wear volume generated at each time instant was divided by the total (both cup and head) wear volume in that walking cycle. In the figure the head wear are added on the top of the cup wear. The highest wear on both components occurred at approximately 40% of the cyclic time, corresponding to the second loading peak. Since there were two loading peaks in one gait cycle, 20% and 40%, taking the non-spherical cup in the last wear cycle for example, if looking into these two loading peaks as highlighted by the red dot in Fig. 7(b), the film thickness contours at these two instants are presented in Fig. 8, in which the location of thinner film thickness distribution are circled out.

To further look at how lubrication influenced the wear at the large time scale of million cycles, the pressure and film thickness were averaged over time in the first and last walking cycle respectively, and these averaged pressure and film thickness distribution along the Medial-Lateral cross-section ( $\theta = 90^\circ$  illustrated as the dash line in Fig. 1) are shown in Fig. 9.

## 6. Discussion

### 6.1. Model validation

The wear results were compared to a previous hip simulator wear test as summaries in Table 2. The predicted wear rates were lower and in the same order of magnitude with the experimental test, while the penetration depth was in one order of magnitude lower.

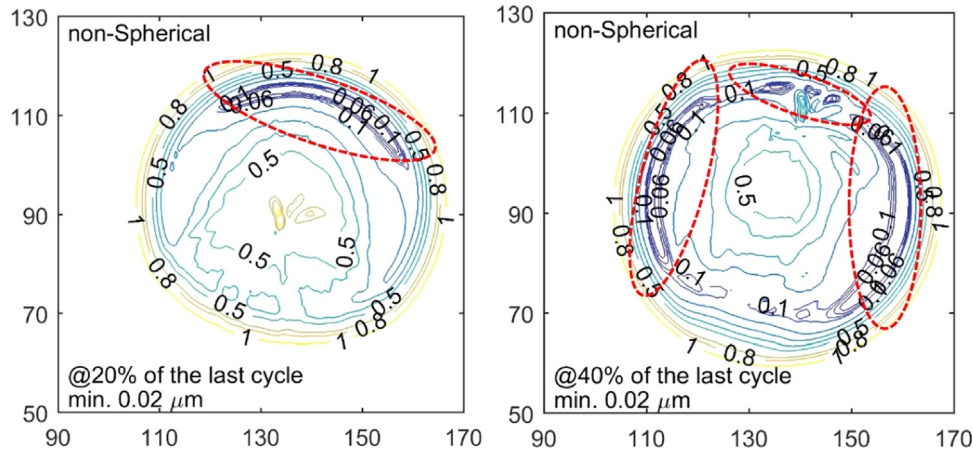


Fig. 8. Film thickness contours of the non-spherical cup at two peak loading time (20% and 40% of cyclic time corresponding to the red dots in Fig. 7(b) in the last wear cycle; locations with thinner film thickness are circled out.

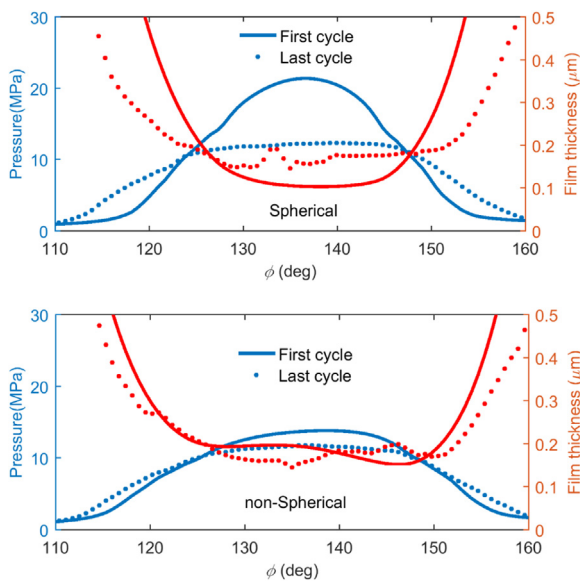


Fig. 9. Averaged pressure and film thickness over cyclic time at the medial-lateral cross-section in a) the spherical and b) the non-spherical hip.

Table 2  
Comparison to a hip simulator wear study [42].

	Al-Hajjar et al. [42]	Current study
Materials	CoCrMo	CoCrMo
Loading and motion cycles	ProSim gait	ProSim gait
cup inclination angle	45°	45°
Cup radius (mm)	36	36
Radial clearance (μm)	20–28.5	25
Ra of cup surface (nm)	16–33	n/a
Ra of head surface (nm)	29–50	n/a
Composite Ra of above (nm)	33–60	40
Running-in wear rate (mm <sup>3</sup> /MC)	0.35	0.08–0.2
Steady-state wear rate (mm <sup>3</sup> /MC)	0.17	0.05–0.08
Maximum penetration depth (μm)	48 (Head); at 3MC	1.04 (Cup); 0.88 (Head); both at 2MC

The numerical wear simulation predicts the wear rate for specimens of ‘perfect’ geometry and materials (e.g., purely spherical geometry and uniformly and isotropic material) under ‘perfect’ ideal conditions (e.g., the loading and motion that are actually output from hip simulators are

not exactly the same as the given curves, while in the numerical models they are). This can explain that in physical joint simulator wear tests, there were generally scatter in wear rate even for same group of specimens. However, it needs to be noted that there are some limitations of the model that could be improved as listed below,

- The constant wear coefficient and the power term of the lambda ratio is not provided by corresponding experimental tests.
- The wear particles playing a role of the third body wear is not taken into account.
- Surface roughness is not considered in the lubrication scale.
- Corrosion accelerated wear (tribocorrosion) is not considered.

As a recent study has pointed out, physical hip simulator wear tests under both ideal and clinical relevant conditions should be used to anticipate clinical performance of hip replacements prior to market release [51]. Severe wear conditions such as edge loading, micro-separation or poor surgical positioning not been addressed are also limitations of the current wear model.

### 6.2. Wear coefficient

The wear coefficient in this study is a power function of the lambda ratio ( $k_w \lambda^{-a}$ ) and basically a function of the lubricated film thickness, which is time-dependent and a distributed field over each bearing surface. Thus the wear coefficient is different for the cup and head surface, and it depends on the composite surface roughness, loading condition, motion, contact geometry and the fluid properties.

If compared with others work in the literature, with the constant wear parameter  $k_w = 2 \times 10^{-8}$  and the  $\lambda$  ratio between 0.5 (at the boundary film thickness of 20 nm) and 3 (full film lubrication), the wear coefficient in our study ranged in  $0.17 \times 10^{-8}$ – $9.45 \times 10^{-8}$ , within the range in the literature which is in the order of magnitude of  $10^{-9}$ – $10^{-8}$  [24,27,31,32,36]. As described in our previous paper, this constant wear parameter ( $k_w$ ) can be grouped together with the number of cycles in the wear formula, and the results are dependent to the product of the  $k_w$  and the number of cycles, independent to the  $k_w$  only by itself.

### 6.3. Surface geometry change and the two-stage wear

The surface profile change during wear led to a change in the gap between the cup and head, which has an important effect on the lubricated film and pressure distribution of hip replacements, and results in the two-stage wear process (except of severe wear conditions). The maximum change of the surface geometry of the metal-on-metal hip

joint in this study, i.e. the sum of maximum wear depth, was  $1.92\ \mu\text{m}$  after 2MC (Fig. 5), and for the fitted non-spherical geometry the maximum depth was  $d = 1.25\ \mu\text{m}$ . This value indicated the effective change to transfer the running-in wear to a steady-state stage. It agrees with what was observed in hip simulator wear tests of MoM hip joints that after 1–2MC the transition of wear stage started [24,41,42]. This change made the head and cup geometries of a more similar local radius (conformity) with a larger contact area. Thus, the distribution of pressure became flatten with a lower maximum pressure value, subjected to the same loading cycle, and the film thickness was increased, which are clearly observed in the spherical hip joint (Fig. 9). The non-spherical hip joint presented a smoother and more evenly distributed wear profile, particularly on the head surface at where the maximum wear depth occurred around  $\theta = 95^\circ$  (Figs. 5 and 6). This location was dependent on the relative motion of the two bearing components.

#### 6.4. Time scale in loading cycles

The real wear process spans in distinct time scales; from chemical reactions between metal surface and synovial fluid in micro-seconds, to the loading cycle of gait in seconds, and to the life time of the joints in years (or for hip simulator tests in months). This study simulated the wear process in two time scales, the gait cycle in seconds and millions of gait cycles representing the life time in years. It is important to understand what loading and motion cycles may cause severe wear. There are two questions to be answered. One is how the wear was reduced in the non-spherical hip from the small cyclic time scale point of view? Despite of the geometry or the wear stage, the highest wear occurred around the second peak loading time in one cycle (Fig. 7). If comparing the steady-state wear to the running-in wear, it can be seen that the highest value of wear was not reduced, on the contrary it was increased. However, the high wear area is narrowed around the second peak loading time resulting in a low accumulated wear. This indicated that an optimal geometry can effectively change the time effect of peak loading, presenting more evenly pressure distribution, particularly when approaching the peak load.

The other question is why there were two loading peaks at 20% and 40% of the cycle time, but the second peak generated much higher wear than the first, independent of the surface geometry or the time scales? This is because the lubrication played an important role and the film thickness varied with squeeze film effect. The minimum film thickness of  $0.02\ \mu\text{m}$  occurred at both instants of 20% and 40% (Fig. 8) which indicated the highest possibility of wear. Although the hip joint was subjected to a similar load at the two time instants, the rotation speed and the squeeze film effect acted differently which resulted in significantly different film thickness field (Fig. 8). It is clear to observe in the film thickness contours that a larger area of low film thickness ( $\lambda < 3$ ) at 40% cyclic time, as circled in Fig. 8, resulted in a much higher wear at this instant than the first loading peak instant.

#### 6.5. Materials

There are concerns of the metal-on-metal hips in terms of the potential toxicity of the metal wear debris to the human body. Although the metal-metal hip implants was employed, the idea in this study may possibly apply to joints made of different materials as the two stage wear trend is observed in other material combinations. Hua et al. [52] studied the contact stress between a worn cup surface and a spherical head using a FE model of metal-on-polyethylene hip joint, and found that a small radial penetration (1–2 mm, representing 10–20 years of service life) resulted in an increased contact area and decreased contact stress. Although, the geometry generated by the penetration of head towards the cup was not an optimal contact geometry, it implied that the non-spherical worn surface contributed to steady-state wear in the metal-on-polyethylene combinations. However, this needs further investigations for each specific material. In clinics the wear performance

of hip joints depends on complicated factors associated with surgery process and patient's specific anatomical and biomechanical characteristics. Despite of the factors from individual differences that affects the wear performance, the surface geometry of the hips is a general factor that could be improved to reduce the running-in wear at lease in the MoM hip joints.

## 7. Conclusions

This paper presented a numerical wear simulation of a MoM non-spherical hip joint and observed a promising 'running-in' free wear performance which resulting in an approximately 50% reduction in the total accumulated wear compared to the corresponding spherical joint. The non-spherical shape for the cup component was inspired by the geometry of the worn profile at steady-state wear stage with low wear rate, observed in many hip simulator and clinical studies. This study presented a 'whole picture' of the lubrication and wear performance; the wear generated against number of gait cycles; the separate wear profiles of the cup and head surfaces and their developments during simulated cycles; in a smaller time scale of one cycle, the wear volume generated at each time instant and the film thickness field at particular time instants. The wear model addressed full lubrication simulation and the wear coefficient was presented as a power function of the  $\lambda$  ratio, which was able to simulate the two-stage wear effectively.

## Acknowledgement

The work was supported by Imperial College Junior Research Fellowship (2015–2018), European Union's Seventh Framework Programme (FP7/2007–2013) under the LifeLongJoints Project (Grant Agreement no. GA-310477), and Shanghai Natural Science Foundation of China (16ZR1411800).

## References

- [1] E. Ebramzadeh, P.A. Campbell, K.M. Takamura, Z. Lu, S.N. Sangiorgio, J.J. Kalma, K.A. De Smet, H.C. Amstutz, Failure modes of 433 metal-on-metal hip implants: how, why, and wear, *Orthop. Clin. N. Am.* (42) (2011) 241–250.
- [2] Z.M. Jin, J. Zheng, W. Li, Z.R. Zhou, *Tribology of medical devices*, *Biosurf. Biotribol.* (2) (2016) 173–192.
- [3] Z.R. Zhou, Z.M. Jin, *Biotribology: recent progresses and future perspectives*, *Biosurf. Biotribol.* (1) (2015) 3–24.
- [4] A.J. Hart, S.A. Sabah, J. Henckel, G. Lloyd, J.A. Skinner, Lessons learnt from metal-on-metal hip arthroplasties will lead to safer innovation for all medical devices, *Hip Int.* (25) (2015) 347–354.
- [5] R.M. Urban, J.J. Jacobs, M.J. Tomlinson, J. Gavrilovic, J. Black, M. Peoc'h, Dissemination of wear particles to the liver, spleen, and abdominal lymph nodes of patients with hip or knee replacement, *J. Bone Jt. Surg.-Am. Vol.* (82A) (2000) 457–477.
- [6] J. Daniel, J. Holland, L. Quigley, S. Sprague, M. Bhandari, Pseudotumors associated with total hip arthroplasty, *J. Bone Jt. Surg.-Am. Vol.* (94A) (2012) 86–93.
- [7] P. Bullough, J. Goodfellow, A.S. Greenwald, J. O'connor, Incongruent surfaces in the human hip joint, *Nature* (217) (1968) 1290.
- [8] F. Menschik, The hip joint as a conchoid shape, *J. Biomech.* (30) (1997) 971–973.
- [9] D.Y. Gu, F. Hu, J.H. Wei, K.R. Dai, Y.Z. Chen, Contributions of non-spherical hip joint cartilage surface to hip joint contact stress, *Conf. Proc. IEEE Eng. Med. Biol. Soc.* 2011 (2011) 8166–8169, <http://dx.doi.org/10.1109/IEMBS.2011.6092014> <<http://www.ncbi.nlm.nih.gov/pubmed/22256237>>.
- [10] F.C. Wang, Z.M. Jin, Effect of non-spherical bearing geometry on transient elastohydrodynamic lubrication in metal-on-metal hip joint implants, *Proc. Inst. Mech. Eng. Part J-J. Eng. Tribol.* (221) (2007) 379–389.
- [11] Q.E. Meng, L.M. Gao, F. Liu, P.R. Yang, J. Fisher, Z.M. Jin, Contact mechanics and elastohydrodynamic lubrication in a novel metal-on-metal hip implant with an aspherical bearing surface, *J. Biomech.* (43) (2010) 849–857.
- [12] J. Fisher, Acetabular Cup, Patent Number: WO95/23566, 1995.
- [13] L.M. Gao, Q.E. Meng, F. Liu, J. Fisher, Z.M. Jin, The effect of aspherical geometry and surface texturing on the elastohydrodynamic lubrication of metal-on-metal hip prostheses under physiological loading and motions, *Proc. Inst. Mech. Eng. Part C-J. Mech. Eng. Sci.* (224) (2010) 2627–2636.
- [14] X.Q. Hu, G.H. Isaac, J. Fisher, Changes in the contact area during the bedding-in wear of different sizes of metal on metal hip prostheses, *Bio-Med. Mater. Eng.* (14) (2004) 145–149.
- [15] A.L. Lippincott, J.B. Medley, Low Wear Ball and Cup Joint Prosthesis, Patent number: WO 97/16138, 1997.
- [16] C. Ernsberger, E. Frazee, Low ion release aspheric metal on metal hip design, in:

- Proceedings of the 54th Annual Meeting of the ORS, 2008.
- [17] C. Ernsberger, E. Frazee, Z. Jin, C. Brockett, Q. Meng, J. Fisher, Lubrication film analysis of an aspheric mom bearing design, in: Proceedings of the 55th Annual Meeting of the ORS, 2009.
- [18] T.D. Brown, H.J. Lundberg, D.R. Pedersen, J.J. Callaghan, Clinical biomechanics of third body acceleration of total hip wear, *Clin. Orthop. Relat. Res.* (467) (2009) 1885–1897.
- [19] R. Lee, A. Essner, A. Wang, Tribological considerations in primary and revision metal-on-metal arthroplasty, *J. Bone Jt. Surg. Am.* 90 (Suppl 3) (2008) S118–S124.
- [20] M.A. Tuke, G. Scott, A. Roques, X.Q. Hu, A. Taylor, Design considerations and life prediction of metal-on-metal bearings: the effect of clearance, *J. Bone Jt. Surg. Am.* 90 (Suppl 3) (2008) S134–S141.
- [21] M. Alvarez-Vera, J.A. Ortega-Saenz, M.A.L. Hernandez-Rodriguez, A study of the wear performance in a hip simulator of a metal-metal Co-Cr alloy with different boron additions, *Wear* (301) (2013) 175–181.
- [22] J.F. Archard, Contact and rubbing of flat surfaces, *J. Appl. Phys.* (24) (1953) 981–988.
- [23] F. Liu, J. Fisher, Z.M. Jin, Computational modelling of polyethylene wear and creep in total hip joint replacements: effect of the bearing clearance and diameter, *Proc. Inst. Mech. Eng. Part J-J. Eng. Tribol.* (226) (2012) 552–563.
- [24] F. Liu, I. Leslie, S. Williams, J. Fisher, Z. Jin, Development of computational wear simulation of metal-on-metal hip resurfacing replacements, *J. Biomech.* (41) (2008) 686–694.
- [25] L. Mattei, F. Di Puccio, B. Piccigallo, E. Ciulli, Lubrication and wear modelling of artificial hip joints: a review, *Tribol. Int.* (44) (2011) 532–549.
- [26] G.K. Sfantos, M.H. Aliabadi, Total hip arthroplasty wear simulation using the boundary element method, *J. Biomech.* (40) (2007) 378–389.
- [27] M.S. Uddin, L.C. Zhang, Predicting the wear of hard-on-hard hip joint prostheses, *Wear* (301) (2013) 192–200.
- [28] L. Gao, D. Dowson, R.W. Hewson, Predictive wear modelling of the metal-on-metal hip replacements, *J. Biomed. Mater. Res.: Part B Appl. Biomater.* (105) (2017) 497–506.
- [29] M.N. Harun, F.C. Wang, Z.M. Jin, J. Fisher, Long-term contact-coupled wear prediction for metal-on-metal total hip joint replacement, *Proc. Inst. Mech. Eng. Part J-J. Eng. Tribol.* (223) (2009) 993–1001.
- [30] L. Kang, A.L. Galvin, J. Fisher, Z.M. Jin, Enhanced computational prediction of polyethylene wear in hip joints by incorporating cross-shear and contact pressure in additional to load and sliding distance: effect of head diameter, *J. Biomech.* (42) (2009) 912–918.
- [31] E. Askari, P. Flores, D. Dabirrahmani, R. Appleyard, Dynamic modeling and analysis of wear in artificial hip articulations, in: Proceedings of the 14th IFToMM World Congress, 2015.
- [32] F. Di Puccio, L. Mattei, A novel approach to the estimation and application of the wear coefficient of metal-on-metal hip implants, *Tribol. Int.* (83) (2015) 69–76.
- [33] F. Liu, J. Fisher, Z.M. Jin, Effect of motion inputs on the wear prediction of artificial hip joints, *Tribol. Int.* (63) (2013) 105–114.
- [34] L. Mattei, F. Di Puccio, Wear simulation of metal-on-metal hip replacements with frictional contact, *J. Tribol.-Trans. ASME* (135) (2013).
- [35] V. Pakhaliuk, A. Polyakov, M. Kalinin, V. Kramar, Improving the finite element simulation of wear of total hip prosthesis' spherical joint with the polymeric component, in: Proceedings of the 25th Daaam International Symposium on Intelligent Manufacturing and Automation, 100, 2014–2015, pp. 539–548.
- [36] M.N. Harun, Z.M. Jin, A. Syahrom, Influence of lubrication performance on wear factor in metal-on-metal hip joint replacement using numerical analysis, in: Proceedings of the International Tribology Conference Malaysia, 68, 2013, pp. 95–101.
- [37] L. Mattei, F. Di Puccio, E. Ciulli, A comparative study of wear laws for soft-on-hard hip implants using a mathematical wear model, *Tribol. Int.* (63) (2013) 66–77.
- [38] L. Mattei, F. Di Puccio, Influence of the wear partition factor on wear evolution modelling of sliding surfaces, *Int. J. Mech. Sci.* (99) (2015) 72–88.
- [39] A. Wang, A. Essner, V.K. Polineni, C. Stark, J.H. Dumbleton, Lubrication and wear of ultrahigh molecular weight polyethylene in total joint replacements, *Tribol. Int.* (31) (1998) 17–33.
- [40] R.M. Hall, A. Unsworth, P. Siney, B.M. Wroblewski, Wear in retrieved charnley acetabular sockets, *Proc. Inst. Mech. Eng. H* (210) (1996) 197–207.
- [41] I. Leslie, S. Williams, C. Brown, G. Isaac, Z.M. Jin, E. Ingham, J. Fisher, Effect of bearing size on the long-term wear, wear debris, and ion levels of large diameter metal-on-metal hip replacements – an in vitro study, *J. Biomed. Mater. Res. Part B-Appl. Biomater.* (87b) (2008) 163–172.
- [42] M. Al-Hajjar, J. Fisher, S. Williams, J.L. Tipper, L.M. Jennings, Effect of femoral head size on the wear of metal on metal bearings in total hip replacements under adverse edge-loading conditions, *J. Biomed. Mater. Res. Part B-Appl. Biomater.* (101b) (2013) 213–222.
- [43] K.J. Sharif, H.P. Evans, R.W. Snidle, D. Barnett, I.M. Egorov, Effect of elastohydrodynamic film thickness on a wear model for worm gears, *Proc. Inst. Mech. Eng. Part J-J. Eng. Tribol.* (220) (2006) 295–306.
- [44] L.M. Gao, F.C. Wang, P.R. Yang, Z.M. Jin, Effect of 3d physiological loading and motion on elastohydrodynamic lubrication of metal-on-metal total hip replacements, *Med. Eng. Phys.* (31) (2009) 720–729.
- [45] D.M. Meyer, J.A. Tichy, Lubrication model of an artificial hip joint: pressure profile versus inclination angle of the acetabular cup, *J. Tribol.-Trans. ASME* (121) (1999) 492–498.
- [46] M.M. Cross, Rheology of non Newtonian fluids: a new flow equation for pseudo-plastic systems, *J. Colloid Interface Sci.* (20) (1965) 417–437.
- [47] L. Gao, D. Dowson, R.W. Hewson, A numerical study of non-Newtonian transient elastohydrodynamic lubrication of metal-on-metal hip prostheses, *Tribol. Int.* (93) (2016) 486–494.
- [48] F.C. Wang, Z.M. Jin, Prediction of elastic deformation of acetabular cups and femoral heads for lubrication analysis of artificial hip joints, *Proc. Inst. Mech. Eng. Part J-J. Eng. Tribol.* (218) (2004) 201–209.
- [49] W.Z. Wang, H. Wang, Y.C. Liu, Y.Z. Hu, D. Zhu, A comparative study of the methods for calculation of surface elastic deformation, *Proc. Inst. Mech. Eng. Part J-J. Eng. Tribol.* (217) (2003) 145–153.
- [50] L. Gao, J. Fisher, Z. Jin, Effect of walking patterns on the elastohydrodynamic lubrication of metal-on-metal total hip replacements, *Proc. Inst. Mech. Eng. Part J-J. Eng. Tribol.* (225) (2011) 515–525.
- [51] J.B. Medley, Can physical joint simulators be used to anticipate clinical wear problems of new joint replacement implants prior to market release? *Proc. Inst. Mech. Eng. Part H-J. Eng. Med.* (230) (2016) 347–358.
- [52] X.J. Hua, B.M. Wroblewski, Z.M. Jin, L. Wang, The effect of cup inclination and wear on the contact mechanics and cement fixation for ultra high molecular weight polyethylene total hip replacements, *Med. Eng. Phys.* (34) (2012) 318–325.